Petroleum Science 20 (2023) 1231–1237

Contents lists available at ScienceDirect

Petroleum Science

journal homepage: www.keaipublishing.com/en/journals/petroleum-science

Original Paper

Active phase morphology engineering of NiMo/Al_2O_3 through La introduction for boosting hydrodesulfurization of 4,6-DMDBT

Ji-Xing Liu [a, b, *], Xiang-Qi Liu [c], Ri-Xin Yan [a], Ling-Feng Jia [b], Hui-Fang Cheng [a], Hui Liu [a], Yan Huang [a], Ming-Qing Hua [a, **], Hua-Ming Li [a], Wen-Shuai Zhu [a, b, ***]

[a] School of Chemistry and Chemical Engineering and Institute for Energy Research, Jiangsu University, Zhenjiang, Jiangsu 212013, China
[b] State Key Laboratory of Heavy Oil Processing and Beijing Key Lab of Oil & Gas Pollution Control, China University of Petroleum, Beijing 102249, China
[c] State Key Laboratory of Fine Chemicals, Dalian University of Technology, Dalian, Liaoning 116024, China

ARTICLE INFO

Article history:
Received 25 May 2022
Received in revised form
12 August 2022
Accepted 21 September 2022
Available online 24 September 2022

Edited by Jia-Jia Fei

Keywords:
NiMo supported Catalyst
$LaAlO_x$ composites
Hydrodesulfurization
Morphology
Reaction kinetics

ABSTRACT

Herein, we designed and constructed a mesoporous $LaAlO_x$ via a solvent evaporation induced self-assembly protocol. The structure and physicochemical property of the corresponding NiMo supported catalyst was analyzed by a set of characterizations, and its catalytic activity was investigated for hydrodesulfurization (HDS) of 4,6-dimethyldibenzothiophene. It has confirmed that the incorporation of La profoundly facilitate the generation of "Type II" NiMoS phase by weakening the interaction of Mo—O—Al leakage and promoting the sulfidation of both Ni and Mo oxides as well as changing the morphology of Ni promoted MoS_2 slabs, thereafter boosting the HDS performance substantially. The finding here may contribute to the fundamental understanding of structure-activity in ultra-deep desulfurization and inspire the advancement of highly-efficient HDS catalyst in future.

1. Introduction

Sulfur oxides (SO_x), originated from the burning of fossil fuels, have caused a series of seriously environmental problems, which attracts extensive attention from the governments around the world (Salazar et al., 2020; Wang et al., 2022). Hydrodesulfurization (HDS) has been the widely used technology to remove the organosulfur compounds in gasoline and diesel (Zheng et al., 2021; Yin et al., 2021). Bimetallic Ni(Co)Mo(W) supported γ-Al_2O_3 has been the extensively used HDS catalyst in industry heretofore (Weise et al., 2021). However, the strong interaction between γ-Al_2O_3 and Ni(Co)Mo(W) oxides not only leads to the generation of "Type I″ Ni(Co)Mo(W)S phase with low stacking number, but also aggravates the formation of inert Ni(Co)S_x and nickel aluminate complexes because Ni(Co) sponsors cannot be effectively implanted in the Mo(W)S_2 slabs (Eijsbouts et al., 2005; Nikulshin et al., 2014; Zhou et al., 2020). As a result, it is still a great challenge for Ni(Co)Mo(W)/γ-Al_2O_3 to achieve ultradeep desulfurization of fuels containing extremely refractory organosulfur compounds, for instance 4,6-dimethyldibenzothiophene (4,6-DMDBT), under relative mild reaction conditions (Zhou et al., 2019). Thus, the design and development of HDS catalyst with superior catalytic activity for the conversion of highly refractory organosulfur compounds has been desirable heretofore.

It has been recognized that the HDS process of highly refractory 4,6-DMDBT mainly involves direct hydrogenolysis desulfurization (DDS) and pre-hydrogenation and desulfurization (HYD) paths (Zheng et al., 2021; Wang et al., 2022; Zhou et al., 2017). Among them, HYD path gets the whip hand by virtue of eliminated steric hindrance effect on the S atom by pre-hydrogenation saturation through the aromatic ring, which allows the free rotation of methyl group on it (Zhou et al., 2018a, b). Therefore, the design and construction of HDS catalysts with superior HYD activity has been thought to be an effective yet straightforward strategy to achieve "zero sulfur" fuels (Tanimu and Alhooshani, 2019). Numerous efforts have been made to tame the electronic and morphology of the

* Corresponding author. School of Chemistry and Chemical Engineering and Institute for Energy Research, Jiangsu University, Zhenjiang, Jiangsu 212013, China.
** Corresponding author.
*** Corresponding author. School of Chemistry and Chemical Engineering and Institute for Energy Research, Jiangsu University, Zhenjiang, Jiangsu 212013, China.
E-mail addresses: jxliu0804@ujs.edu.cn (J.-X. Liu), huamq840710@163.com (M.-Q. Hua), zhuws@ujs.edu.cn (W.-S. Zhu).

https://doi.org/10.1016/j.petsci.2022.09.023

active phase over bimetallic Ni(Co)Mo(W) supported γ-Al_2O_3 to enhance the HYD activity of HDS catalysts by the modification of Ga, Ti, Mn, Mg, SiO_2, etc., and great progresses have been made (Chen et al., 2017; Zhou et al., 2017, 2020; Muhammad et al., 2019; Nadeina et al., 2018) in the past decade years. Zhou and coauthors prepared series of Ti modified mesoporous NiMo/Al_2O_3 catalysts and found that the incorporation of Ti effectively regulated the acid center and acid strength, thereafter inhibiting the formation of strong Al–O–Mo bond, and thereby promoting the generation of "Type II" NiMoS active phase and the HDS activities of catalysts for 4,6-DMDBT conversion (Zhou et al., 2020). Nadeina and coauthors claimed that the addition of Mg could effectively tailor the acidic and alkaline sites on carrier surface and suppress the polymerization of molybdenum species, thereafter improving the performance of HDS catalyst for 4,6-DMDBT (Nadeina et al., 2018). Nevertheless, it has to be noted that these complexes modified by the introduction of the above metals or nonmetals into Al_2O_3 are formed by the weak electronic interaction. As a result, it usually needs too much additive to modulate the morphology of active phase over HDS catalysts to obtain the optimal catalytic performance. Moreover, the introduction of the above additives usually induces the notable change of pore structure of Al_2O_3 except the morphology of NiMoS active phase (Zhou et al., 2020; Lebeau et al., 2020). Therefore, how the structure of NiMoS active phase influences the catalytic activities of HDS catalysts towards 4,6-DMDBT conversion, however, remains a matter of debate. Toward this end, the design and development of novel catalyst possessing stronger electronic interaction and excellent catalytic performance for HDS is highly desirable.

Herein, we introduce a facile solvent evaporation-induced self-assembly approach to fabricate a mesoporous $LaAlO_x$ binary oxide with low La doping amount (1.0 wt%), and its corresponding NiMo (12.0 wt% MoO_3 and 4.0 wt% NiO) supported $LaAlO_x$ sample was prepared by an improved wetness incipient impregnation method. The structural and physicochemical property of resultant support and NiMo supported catalyst were characterized by powder X-ray diffraction (XRD), nuclear magnetic resonance aluminum spectroscopy (Al MAS NMR) and N_2 adsorption-desorption. The effect of La incorporation on metal-support interaction (MSI) of catalyst and thereafter the formation of catalyst active phase morphology as well as "Type II" NiMoS active phase was analyzed by H_2 temperature programmed reduction (H_2-TPR), pyridine adsorption Fourier transform infrared spectroscopy (Py-FTIR), X-ray photoelectron spectroscopy (XPS) and high-resolution transition electron microscopy (HRTEM). The catalytic activity of NiMo/$LaAlO_x$ was investigated for HDS of 4,6-DMDBT.

2. Experimental

2.1. Preparation of catalysts

Mesoporous $LaAlO_x$ oxides with 1.0 wt% La mass contents were fabricated through an enhanced solvent evaporation induced self-assembly method. During preparation, P123 (average Mn-5800) serving as structure directing agent, $La(NO_3)_3\cdot 6H_2O$ (99%) as lanthanum source, Al(O-i-Pr)$_3$ (99.99%) as aluminum source. Ethanol absolute (EtOH, 98%) as solvent. The typical procedure is described as follows: first, 8.2 g of Al(O-i-Pr)$_3$ was dispersed in a three-necked flask with 20 mL of EtOH and stirred for 4 h followed by the introduction of 3.2 mL of HNO_3 (> 68.0%) within 10 min and stirred for another 0.5 h. Then 4.0 g of P123 was completely dissolved into 20 mL absolute ethanol and slowly dropwise into the aforementioned solution and continue stirring for another 2 h. Finally, a certain quality of $La(NO_3)_3\cdot 6H_2O$ was subsequently dissolved into 10 mL of absolute ethanol and then introduced into the above solution to obtain the precursor solution after 12 h. Then $LaAlO_x$ binary oxide was obtained by drying the above precursor solution at 120 °C for two days and calcinating at 550 °C in air for 4 h.

Bimetallic NiMo/$LaAlO_x$ was fabricated by a wetness incipient impregnation method. In a typical preparation, a certain volume of deionized water solution containing calculated amount of $Ni(NO_3)_2\cdot 6H_2O$ (> 99.8%) and $(NH_4)_6Mo_7O_{24}\cdot 4H_2O$ (> 99.8%) was dropwise to the 1.0 g of as-prepared $LaAlO_x$ binary oxide powders followed by drying and calcining at 120 °C in air for 6 h. Finally, NiMo/$LaAlO_x$ catalyst with 12.0 wt% MoO_3 and 4.0 wt% NiO was obtained by calcining the above precursor powders at 550 °C in air for 4 h.

2.2. Catalytic performance assessment

The HDS activity of NiMo/$LaAlO_x$ binary oxide for 4,6-DMDBT conversion was evaluated in a fixed bed downflow stainless steel reactor (400 mm in length inner and 10 mm in diameter). First, 0.30 g of sample with 20–40 mesh was fully diluted with an equal amount of quartz sand to reach a total volume of 2 mL followed by loading it into the middle of this reactor. The upper and lower ends of reactor were filled with the same volume of quartz sand. Then 3.0 wt% CS_2 solution in cyclohexane was in situ pre-sulfurized over the catalyst at 360 °C for 12 h under 4 MPa of H_2 pressure. The CS_2 cyclohexane solution was then converted to a model oil containing 500 ppm 4,6-DMDBT in dodecane and the vulcanization temperature was reduced to 340 °C. The model oil passes through the catalyst at liquid space-time velocity (LHSV) of 5.0 h^{-1} with H_2/feed volume ratio of 400. The reaction rate constant of NiMo/$LaAlO_x$ catalyst for HDS of 4,6-DMDBT at 340 °C was estimated based on the following equations (Mei et al., 2022; Hu et al., 2022):

$$k_{HDS} = F\cdot \mathrm{In}(1/1-\tau)/m \tag{1}$$

$$k_{DDS} = k_{HDS}\cdot S_{DDS} \tag{2}$$

$$k_{HYDS} = k_{HDS} - k_{DDS} \tag{3}$$

wherein, τ stands for the 4,6-DMDBT concentration in the final product, F is the molar flow rate of 4,6-DMDBT, m is the mass of the catalyst, and S_{DDS} represent the selectivity for 3,3′-DMDBT. When the 4,6-DMDBT conversion is lower than 15% though taming the LHSV, the turnover frequency (TOF) of 4,6-DMDBT at 340 °C was calculated based on Eq. (4):

$$TOF = F\cdot\tau/n_{Mo}\cdot f_{Mo} \tag{4}$$

In Eq. (4), n_{Mo} represents the molar amount of Mo atom in the catalyst, τ stands for the 4,6-DMDBT conversion, F is the molar flow rate of 4,6-DMDBT. Based on the established equation, the dispersion degree (f_{Mo}) of Mo species is evaluated based on the following equation (Zhou et al., 2017; Fan et al., 2011):

$$f_{Mo} = Mo_e \Big/ Mo_t = \sum_{i=1}^{t} 6(n_i-1) \Big/ \sum_{i=1}^{t}\left(3n_i^2 i - 3n_i + 1\right) \tag{5}$$

In Eq. (5), t represents the statistic number of MoS_2 slab evaluated for more than 1000 Ni promoted MoS_2 slab; Mo_e is the number of Mo atoms at the edge and Mo_t is the total number of Mo atoms on MoS_2 slab; n_i stands for the number of Mo atoms along the edge of MoS_2 slab and obtained based on the following equation (Cao et al., 2020):

$$(L = 3.2(2n_i - 1)\text{Å}) \quad (6)$$

According to the formula reported in literature, at least 1000 MoS_2 slabs were counted, and the average slab length and average stacking number were estimated based on the following equations (Wu et al., 2020):

$$\text{Average slab length: } \bar{L} = \sum_{i=1}^{n} n_i l_i \Big/ \sum_{i=1}^{n} ni \quad (7)$$

$$\text{Average stack number: } \bar{N} = \sum_{i=1}^{n} n_i N_i \Big/ \sum_{i=1}^{n} n_i \quad (8)$$

In Eqs. (7) and (8), N_i is the number of layers in slab i, n_i and l_i are the number of MoS_2 slab of length and slab length, respectively.

3. Results and discussion

The phase composition of as-fabricated $LaAlO_x$ support was first investigated by XRD (Fig. 1A). Several distinct characteristic diffraction peaks are noted at 2θ = 19.58, 37.60, 45.78, 60.46 and 66.76°, which could be assigned to γ-Al_2O_3 (PDF#10−0425) (Muhammad et al., 2019), Moreover, no characteristic diffractions assigned to LaO_x are detected (Feng et al., 2019) on $LaAlO_x$ sample. It reveals that the introduction of La species doesn't distinctively influence the pristine γ-Al_2O_3 structure and that the La species is well dispersed on the surface or inside the architecture of mesoporous γ-Al_2O_3. To figure out the chemical state of incorporated La species in the structure of mesoporous γ-Al_2O_3, Al MAS NMR characterization was performed for Al_2O_3 and $LaAlO_x$ samples (Fig. S1). The relative ratio of various coordinate aluminum species based on their corresponding integral areas in NMR spectra was calculated and depicted in Fig. 1B. The aluminum species with four coordination increases notably from 24.0% to 28.0%. In sharp contrast, the aluminum species with six coordination apparently decreases from 32.0% to 26.8% instead with the incorporation of 1.0 wt% of La compared with pristine γ-Al_2O_3. It indicates that the incorporated La species may interact with the six coordinated aluminum species in γ-Al_2O_3 to form the precursor of $LaAlO_3$ perovskite, thereafter resulting in the decline of six coordinated aluminum and the increase of four coordinated aluminum species in $LaAlO_x$ binary oxide. The highly distribution of different coordination form of Al species in $LaAlO_x$ were confirmed by EDS mapping (Fig. 1C). Hence, in view of the above observation, it can be inferred that the introduction of La species by this *in-situ* doping strategy significantly affects the coordination form of Al, thereafter regulating the electronic structure of Al^{3+} species on surface of $LaAlO_x$ binary oxide, which may influence the MSI.

To probe the effect of different coordination form of Al species on the distribution of active metal oxides over NiMo/$LaAlO_x$ catalyst, we performed XRD (Fig. S2). Note that both NiMo/Al_2O_3 and NiMo/$LaAlO_x$ show the characteristic diffraction peaks attributed to γ-Al_2O_3, and no diffractions ascribed to NiO and MoO_3 were observed (van Haandel et al., 2015). It indicates that NiO and MoO_3 species are well dispersed on the surfaces of $LaAlO_x$ and that the introduction of La species may not distinctively influence the dispersion of NiO and MoO_3 on $LaAlO_x$. To further get insight into the effect of La introduction on distribution of active metal oxides over NiMo/$LaAlO_x$ catalyst, we recorded ultraviolet visible diffuse reflectance spectroscopy (UV-Vis DRS). Note that a perceptible blue shift in the absorption bands (Fig. S3A) of Mo species corresponding to different coordination states is noted for NiMo/$LaAlO_x$ compared with NiMo/Al_2O_3. The E_g value (Fig. S3B) of NiMo/$LaAlO_x$ was calculated to be 2.72 eV, which is notably larger than that of NiMo/Al_2O_3. It reveals that the incorporation of 1.0 wt% of La significantly influence the distribution of active metal oxides on NiMo/$LaAlO_x$. The larger E_g value the catalyst exhibits, the higher dispersion of

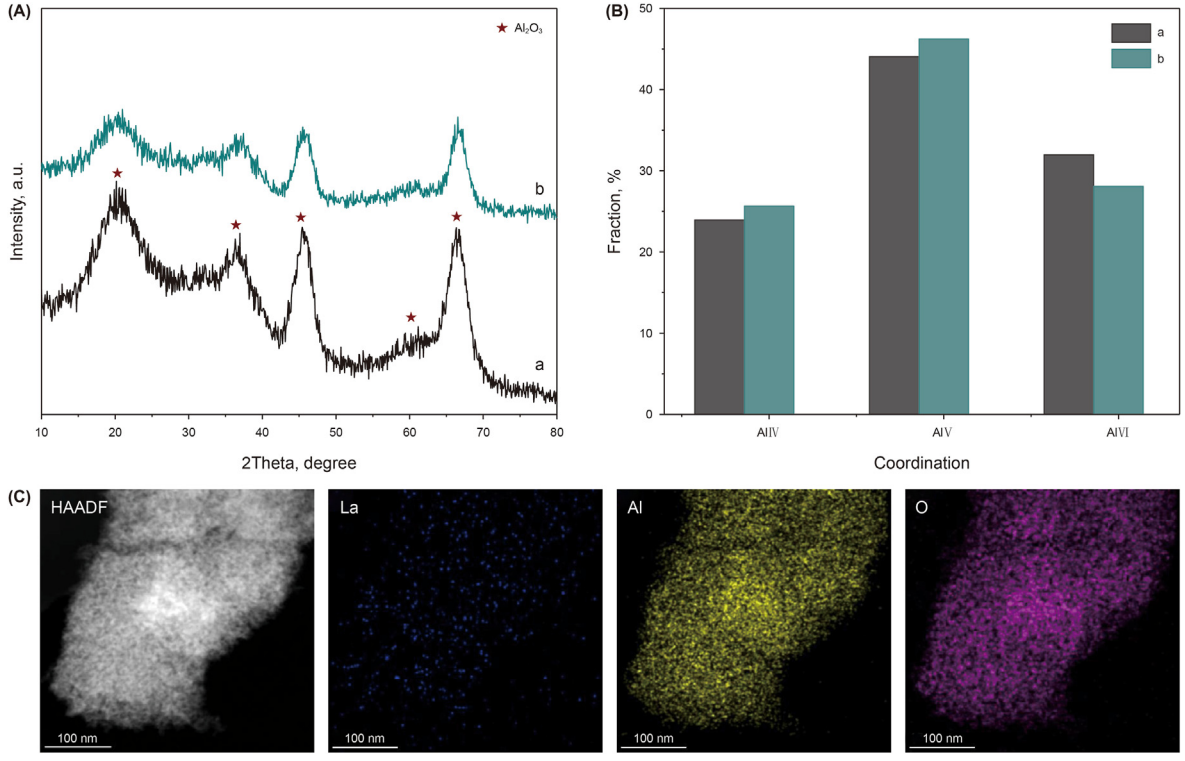

Fig. 1. (**A**) XRD patterns, (**B**) the percentage of coordinated aluminum species in Al MAS NMR of the supports: (a) Al_2O_3, (b) $LaAlO_x$ and (**C**) EDS mapping images of $LaAlO_x$.

active metal oxide NPs the catalyst shows, the more active sites the catalyst exposes (Shan et al., 2015; Liu et al., 2020). It may be beneficial to enhancing the HDS performance of NiMo/$LaAlO_x$ for 4,6-DMDBT.

In order to study how La addition affects the pore structure of synthetic material, we conducted N_2 physical adsorption-desorption experiments for NiMo/Al_2O_3 and NiMo/$LaAlO_x$ catalysts. As plotted in Fig. 2A, both the NiMo/Al_2O_3 and NiMo/$LaAlO_x$ catalysts show type IV N_2 isotherms with H1 type hysteresis loops in the relative pressure of 0.40–0.80 (Naboulsi et al., 2017). In addition, the position of hysteresis loop does not change profoundly with the incorporation of La. It indicates the presence of well-defined mesopore structures of NiMo/$LaAlO_x$ and that the introduction of La does not influence the pore structure of γ-Al_2O_3. It matches well with the pore size distribution result shown in Fig. 2B.

To further study the effect of La introduction on MSI of NiMo/$LaAlO_x$ catalyst, we carried out H_2 temperature programmed reduction (H_2-TPR) experiments. As illustrated in Fig. 2C, both NiMo/Al_2O_3 and NiMo/$LaAlO_x$ show two apparent H_2 consumption peaks corresponding to the MoO_3 reduction to MoO_2 and the MoO_2 reduction to Mo in the region of 200–900 °C, respectively (van Haandel et al., 2020). Notably, NiMo/$LaAlO_x$ exhibits a distinct lower reduction temperature compared with NiMo/Al_2O_3. It indicates that the low amount of La doping could effectively weaken the MSI, which may favour the active phase transition from MoO_3 to "Type II" NiMoS active phase during vulcanization, thereby promoting the HDS activity of catalyst for 4,6-DMDBT conversion. To further study the effect of La introduction on the MSI of NiMo/$LaAlO_x$ catalyst, we collected pyridine adsorption Fourier transform infrared (Py-FTIR) spectra at 350 °C (Fig. 2C). With the introduction of La, the medium-strong acid sites over NiMo/$LaAlO_x$ (Table S1) decline perceptibly compared with that of NiMo/Al_2O_3. It indicates that the incorporation of La perceptibly decrease the acid strength of NiMo/$LaAlO_x$ catalyst, which thereafter weaken the MSI and promote the sulfidation of both Mo and Ni species, and thereby improving HDS activity of the corresponding sulfide catalyst.

It has been recognized that the morphology of Ni promoted MoS_2 slab significantly influences the HDS activity of corresponding catalyst for the removal highly refractory organosulfur compounds with steric hindrance (Shan et al., 2015; Hensen et al., 2001). Thus, the effect of La introduction on the morphology of Ni promoted MoS_2 slab over NiMo/$LaAlO_x$ catalyst was investigated by HRTEM. As depicted in Fig. 3, the single and double stacking number of short MoS_2 slabs promoted by Ni are observed on pristine NiMo/Al_2O_3 catalyst. After the incorporation of 1.0 wt% La, the average slab length and stacking number of MoS_2 slabs promoted by Ni increase considerably from 2.8 nm to 3.2 nm and 1.4 to 2.7, respectively. This results in a slight decrease (from 0.26 to 0.24) in the occupancy of the Mo atoms in edge positions compared with NiMo/Al_2O_3. It indicates that the incorporation of 1.0 wt% of La profoundly influences the morphology of NiMoS active phase over NiMo/$LaAlO_x$ catalyst. It has been well-established that the proper lengthening of Ni promoted MoS_2 slab could promote the HDS activity of sulfide catalyst for 4,6-DMDBT conversion, because the activity of DDS pathway of HDS catalysts is positively associated with the Mo atoms at corner positions, and the HYD pathway is strongly related to the Mo atoms at edge sites (Toulhoat, 2021).

It has been widely-documented that the chemical states of promoter Ni species and Mo species significantly influence the generation of "Type II" NiMoS active phases (Nadeina et al., 2018; Zheng et al., 2020). Therefore, XPS was conducted to investigate the chemical states of Ni and Mo species on sulfide NiMo/Al_2O_3 and NiMo/$LaAlO_x$ samples. The Mo 3d XPS of sulfide NiMo/$LaAlO_x$ sample is illustrated in Fig. S4A, and the relative proportion of Ni and Mo species were summarized in Table S3. Note that the sulfidation degree of NiMo/$LaAlO_x$ is 68.2%, which is higher than that of NiMo/Al_2O_3 (59.1%). This matches well with the H_2-TPR and Py-FTIR

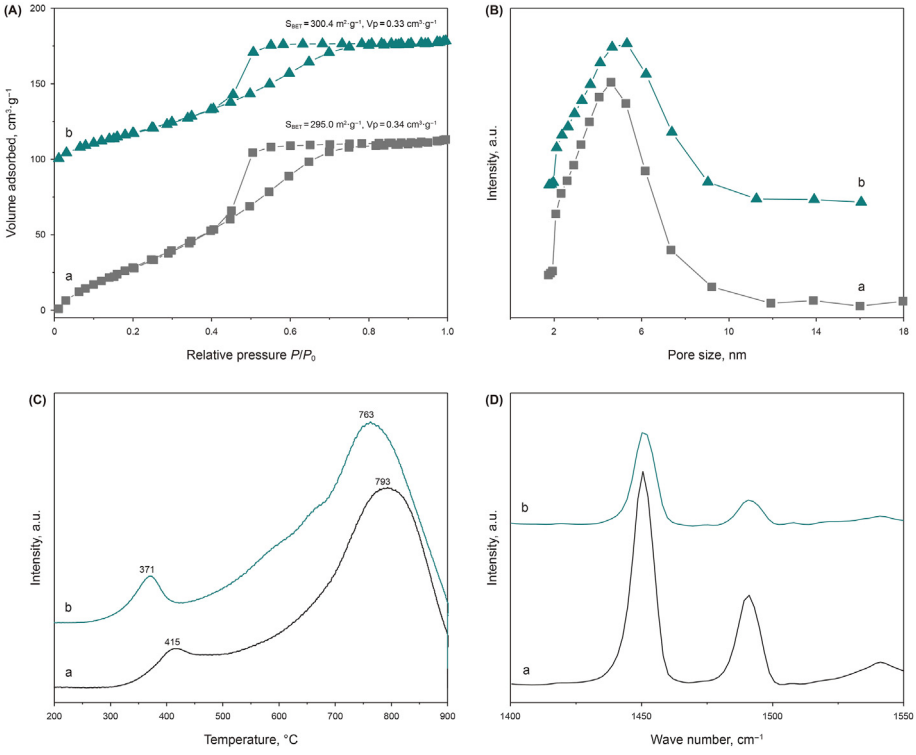

Fig. 2. (**A**) N_2 adsorption-desorption isotherms, (**B**) Pore size distributions, (**C**) H_2-TPR profiles and (**D**) Py-FTIR spectra of the catalysts: (a) NiMo/Al_2O_3 and (b) NiMo/$LaAlO_x$.

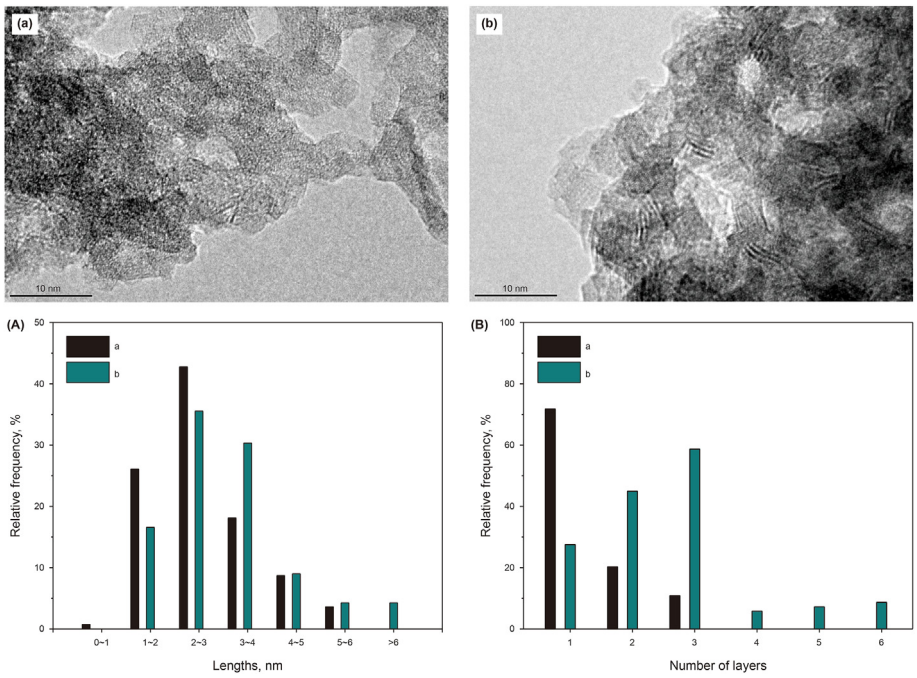

Fig. 3. Distributions of the slab lengths (**A**) and stacking numbers (**B**) of MoS_2 slabs on sulfide catalysts: (a) NiMo/Al_2O_3 and (b) NiMo/$LaAlO_x$.

observations. Moreover, note that the ratio of NiMoS phases over NiMo/$LaAlO_x$ (76.1%) increases perceptibly compared to that of NiMo/Al_2O_3 (66.1%). It reveals that the introduction of 1.0 wt% La into Al_2O_3 substantially facilitate the sulfurization of Ni species to generate NiMoS active phase.

Combined with the above results, the incorporation of 1.0 wt% of La could effectively tame the morphology of NiMoS active phase over NiMo/LaAlOx catalyst. The effect of La introduction on the catalytic activity of NiMo supported sample was investigated for 4,6-DMDBT HDS. As illustrated in Fig. 4, the 4,6-DMDBT conversion over NiMo/$LaAlO_x$ is about 96.0%, which is perceptible higher than that of pristine NiMo/Al_2O_3 (61.0%). This is in accordance with the change trend of MSI and the proportion of NiMoS active phase. It indicates that the above two factors are positively associated with the catalytic activity of NiMo/$LaAlO_x$ for 4,6-DMDBT HDS.

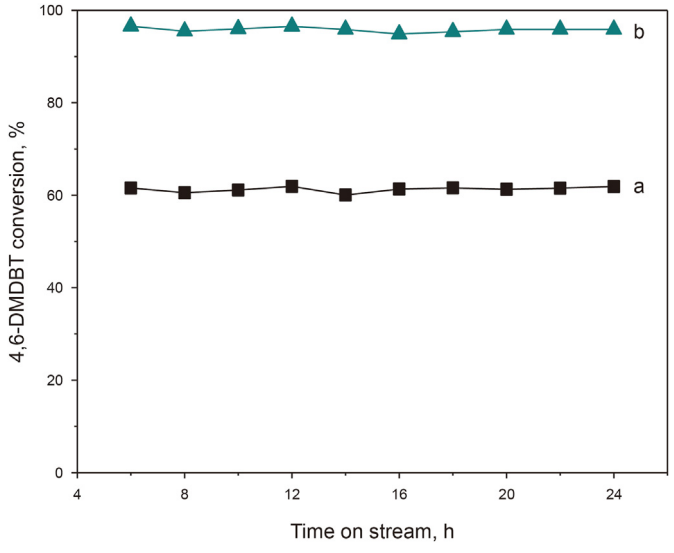

Fig. 4. The 4,6-DMDBT conversion over the catalysts: (a) NiMo/Al_2O_3 and (b) NiMo/$LaAlO_x$.

To deeply probe the intrinsic cause of La introduction on the above activity result, we compared the product distribution of NiMo/Al_2O_3 and NiMo/$LaAlO_x$ catalysts for 4,6-DMDBT conversion (~50%) by means of GC-MS (Table S4). Note that the introduction of 1.0 wt% of La could significantly promote HYD path of NiMo/$LaAlO_x$ catalyst, which should be the original reason leading to the considerable enhancement for 4,6-DMDBT conversion over NiMo/$LaAlO_x$.

To further get insight into the HDS activity of NiMo/$LaAlO_x$ sample in more detail, the overall reaction rate constants of 4,6-DMDBT HDS over NiMo/Al_2O_3 and NiMo/$LaAlO_x$ were calculated (Table 1). Note that the overall rate constant of NiMo/$LaAlO_x$ catalyst is 13.7 $\times$ 10^{-6} mol g^{-1} s^{-1}, which is 1.85 times that of NiMo/Al_2O_3 (7.4 $\times$ 10^{-6} mol g^{-1} s^{-1}). It indicates that the introduction of 1.0 wt% of La into mesoporous Al_2O_3 could effectively improve the catalytic activities of corresponding NiMo supported catalysts. Since this class of catalyst has two parallel paths towards the HDS of 4,6-DMDBT. The detailed kinetic parameters of NiMo/$LaAlO_x$ for 4,6-DMDBT HDS was estimated based on the reaction network (Fig. S5). As exhibited in Table 1, the reaction rate constant belonging to HYDS reaction path over NiMo/$LaAlO_x$ (13.0 $\times$ 10^{-6} mol g^{-1} s^{-1}) is significantly enhanced compared with that of NiMo/Al_2O_3 (6.8 $\times$ 10^{-6} mol g^{-1} s^{-1}), while both NiMo/Al_2O_3 and NiMo/$LaAlO_x$ exhibit the similar reaction rate constants corresponding to DDS reaction path. It unveils that the main factor responsible for the change in overall reaction rate constant is the variation in the HYDS pathway. For a more explicit comparison, the TOF at the active edge sites of NiMo/$LaAlO_x$ was calculated. Note that the TOF value of pristine NiMo/Al_2O_3 catalyst is only 2.1 h^{-1}. After the incorporation of 1.0 wt% of La into mesoporous Al_2O_3, the TOF value increases significantly to 3.5 h^{-1} over NiMo/$LaAlO_x$.

Combined with the above observations, it could be concluded that the incorporation of 1.0 wt% La considerably influences the electronic structure of Al^{3+} species on the surface of $LaAlO_x$ binary oxides by the interaction with the six coordinated aluminum

Table 1
The kinetic parameters of sulfide NiMo supported catalysts for 4,6-DMDBT HDS.

Catalyst	k_{HDS}, mol g^{-1} s^{-1}	TOF, h^{-1}	k_{HYDS}, mol g^{-1} s^{-1}	k_{DDS}, mol g^{-1} s^{-1}
$NiMo/Al_2O_3$	7.4×10^{-6}	2.1	6.7×10^{-6}	6.6×10^{-6}
$NiMo/LaAlO_x$	13.7×10^{-6}	3.5	13.0×10^{-6}	7.0×10^{-6}

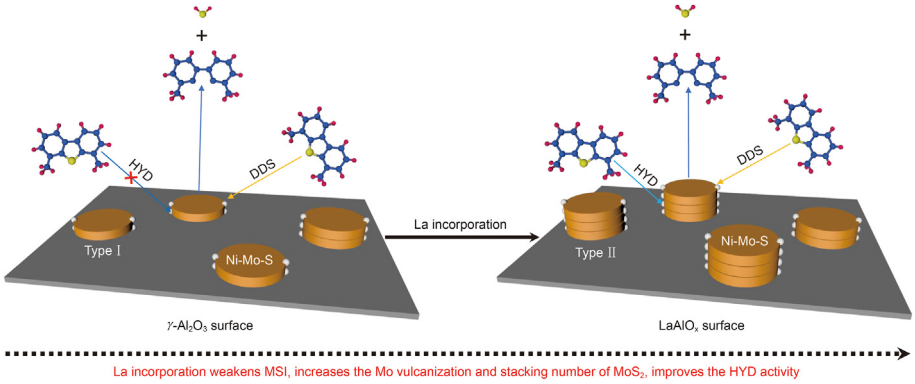

Scheme 1. Illustration of the effect of La incorporation on the support property, active phase morphology and reaction pathway of $NiMo/Al_2O_3$ for 4,6-DMDBT conversion.

species in γ-Al_2O_3 to form the precursor of $LaAlO_3$ perovskite, thereafter weakening the strong interaction between active metal oxides and γ-Al_2O_3, that is Mo–O–Al band, significantly, which is subsequently confirmed by the H_2-TPR and Py-FTIR results, and thereby promoting the reduction of MoO_3 as well as favoring the active phase transition from MoO_3 to "Type II" NiMoS active phase during vulcanization. The sulfidation of both Mo and Ni species as well as the proportion of "Type II" NiMoS active phase are notably enhanced. In other words, the morphology of NiMoS active phase was engineered by this low amount of La introduction. As a result, the HYD and overall reaction rate constants for 4,6-DMDBT HDS over $NiMo/LaAlO_x$ are remarkable increased compared with the pristine $NiMo/Al_2O_3$ (as depicted in Scheme 1).

4. Conclusions

In summary, we have successfully fabricated a mesoporous $NiMo/LaAlO_x$ through a solvent evaporation induced self-assembly strategy. The catalytic activity of $NiMo/LaAlO_x$ for 4,6-DMDBT HDS was systematically investigated. It was found that the addition of La significantly influence the morphology and electronic structure of NiMoS active phase. The low amount of La doping notably facilitates the formation of "Type II" NiMoS phase by weakening the interaction of Mo–O–Al leakage and promoting the vulcanization of Ni and Mo species as well as changing the morphology of MoS_2 slabs promoted by Ni, thereby boosting the HDS performance substantially by the facilitated NiMoS active phase and HYD route. Therefore, this present study may be beneficial for deeply understanding, design and preparation of highly efficient ultra-deep HDS catalyst in future.

Declaration of competing interest

The authors declare no competing financial interest.

Acknowledgements

The authors thank the financial support of the National Natural Science Foundation of China (22002050, 22178154), the Project of Jiangsu University Senior Talents Foundation (20JDG35), Postdoctoral Science Foundation of China (2022T150765, 2020M683154) and National Engineering Laboratory for Mobile Source Emission Control Technology (NELMS2020B01).

Appendix A. Supplementary data

Supplementary data to this article can be found online at https://doi.org/10.1016/j.petsci.2022.09.023.

References

Chen, W., Long, X., Li, M., Nie, H., Li, D., 2017. Influence of active phase structure of $CoMo/Al_2O_3$ catalyst on the selectivity of hydrodesulfurization and hydrodearomatization. Catal. Today 292, 97–109. https://doi.org/10.1016/j.cattod.2016.09.029.

Cao, Z.K., Guo, R., Du, P., Mei, J., Zhang, X., Xu, C., Liu, J., Jiang, G., Li, H., Duan, A.J., 2020. Synthesis of highly ordered Al-Zr-SBA-16 composites and their application in dibenzothiophene hydrodesulfurization. Chem. Eng. Sci. 13, 115415. https://doi.org/10.1016/j.ces.2019.115415.

Eijsbouts, S., van den Oetelaar, L.C.A., van Puijenbroek, R.R., 2005. MoS_2 morphology and promoter segregation in commercial Type 2 $Ni-Mo/Al_2O_3$ and $Co-Mo/Al_2O_3$ hydroprocessing catalysts. J. Catal. 229, 352–364. https://doi.org/10.1016/j.jcat.2004.11.011.

Feng, S., Lin, X., Song, X., Liu, Y., Jiang, Z., Ding, Y., 2019. Insight into the stability of binuclear Ir-La catalysts for efficient heterogeneous methanol carbonylation. J. Catal. 377, 400–408. https://doi.org/10.1016/j.jcat.2019.06.050.

Fan, Y., Xiao, H., Shi, G., Liu, H., Bao, X., 2011. A novel approach for modulating the morphology of supported metal nanoparticles in hydrodesulfurization catalysts. Energy Environ. Sci. 4 (2), 572–582. https://doi.org/10.1039/C0EE00379D.

Hensen, E.J.M., Kooyman, P.J., van der Meer, Y., Van der Kraan, A.M., De Beer, V.H.J., Van Veen, J.A.R., Van Santen, R.A., 2001. The relation between morphology and hydrotreating activity for supported MoS_2 particles. J. Catal. 199, 224–235. https://doi.org/10.1006/jcat.2000.3158.

Hu, D., Li, H.P., Mei, J.L., Xiao, C.K., Wang, E.H., Chen, X.Y., Zhang, W.X., Duan, A.J., 2022. The effect of chelating agent on hydrodesulfurization reaction of ordered mesoporous alumina supported NiMo catalysts. Petrol. Sci. 19 (1), 321–328. https://doi.org/10.1016/j.petsci.2021.11.005.

Lebeau, B., Bonne, M., Comparot, J.D., Rousseau, J., Michelin, L., Blin, J.L., Brunet, S., 2020. HDS of 4,6-dimethyldibenzothiophene over CoMoS supported mesoporous SiO_2-TiO_2 materials. Catal. Today 357, 675–683. https://doi.org/10.1016/j.cattod.2019.02.052.

Liu, Z., Han, W., Hu, D., Sun, S., Hu, A., Wang, Z., Jia, Y., Zhao, X., Yang, Q., 2020. Effects of Ni-Al_2O_3 interaction on $NiMo/Al_2O_3$ hydrodesulfurization catalysts. J. Catal. 387, 62–72. https://doi.org/10.1016/j.jcat.2020.04.008.

Mei, J.L., Shi, Y., Xiao, C.K., Wang, A.C., Duan, A.J., Wang, X.L., 2022. Hierarchically porous Beta/SBA-16 with different silica-alumina ratios and the hydrodesulfurization performances of DBT and 4,6-DMDBT. Petrol. Sci. 19 (1), 375–386. https://doi.org/10.1016/j.petsci.2021.10.003.

Muhammad, Y., Rashid, H.U., Subhan, S., Rahman, A.U., Sahibzada, M., Tong, Z.F.,

2019. Boosting the hydrodesulfurization of dibenzothiophene efficiency of Mn decorated (Co/Ni)-Mo/Al_2O_3 catalysts at mild temperature and pressure by coupling with phosphonium based ionic liquids. Chem. Eng. J. 375, 121957. https://doi.org/10.1016/j.cej.2019.121957.

Naboulsi, I., Aponte, C.F.L., Lebeau, B., Brunet, S., Michelin, L., Bonne, M., Blin, J.L., 2017. An unexpected pathway for hydrodesulfurization of gazole over a CoMoS active phase supported on a mesoporous TiO_2 catalyst. Chem. Commun. 53, 2717–2720. https://doi.org/10.1039/C7CC00848A.

Nadeina, K.A., Klimov, O.V., Danilova, I.G., Pereyma, V.Y., Gerasimov, E.Y., Prosvirin, I.P., Noskov, A.S., 2018. Amorphous silica-alumina-perspective supports for selective hydrotreating of FCC gasoline: influence of Mg. Appl. Catal. B Environ. 223, 22–35. https://doi.org/10.1016/j.apcatb.2017.07.004.

Nikulshin, P.A., Salnikov, V.A., Mozhaev, A.V., Minaev, P.P., Kogan, V.M., Pimerzin, A.A., 2014. Relationship between active phase morphology and catalytic properties of the carbon alumina-supported Co(Ni)Mo catalysts in HDS and HYD reactions. J. Catal. 309, 386–396. https://doi.org/10.1016/j.jcat.2013.10.020.

Salazar, N., Rangarajan, S., Rodriguez-Fernandez, J., Mavrikakis, M., Lauritsen, J.V., 2020. Site-dependent reactivity of MoS_2 nanoparticles in hydrodesulfurization of thiophene. Nat. Commun. 11 (1), 1–9. https://doi.org/10.1038/s41467-020-18183-4.

Shan, S., Yuan, P., Han, W., Shi, G., Bao, X., 2015. Supported NiW catalysts with tunable size and morphology of active phases for highly selective hydrodesulfurization of fluid catalytic cracking naphtha. J. Catal. 330, 288–301. https://doi.org/10.1016/j.jcat.2015.06.019.

Tanimu, A., Alhooshani, K., 2019. Advanced hydrodesulfurization catalysts: a review of design and synthesis. Energy Fuel. 33 (4), 2810–2838. https://doi.org/10.1021/acs.energyfuels.9b00354.

Toulhoat, H., 2021. A perspective on the catalytic hydrogenation of aromatics by Co(Ni)MoS phases. J. Catal. 403, 121–130. https://doi.org/10.1016/j.jcat.2021.01.020.

van Haandel, L., Bremmer, M., Kooyman, P.J., van Veen, J.A.R., Weber, T., Hensen, E.J.M., 2015. Structure-activity correlations in hydrodesulfurization reactions over Ni-promoted $Mo_xW(1-x)$/Al2O3 catalysts. ACS Catal. 5, 7276–7287. https://doi.org/10.1021/acscatal.5b01806.

van Haandel, L., Smolentsev, G., van Bokhoven, J.A., Hensen, E.J.M., Weber, T., 2020. Evidence of octahedral Co-Mo-S sites in hydrodesulfurization catalysts as determined by resonant inelastic X-ray scattering and X-ray absorption spectroscopy. ACS Catal. 10 (19), 10978–10988. https://doi.org/10.1021/acscatal.0c03062.

Wang, B., Chen, Z., Jiang, T., Yu, J., Yang, H., Duan, A.J., Xu, C., 2022. Restrictive diffusion and hydrodesulfurization reaction of dibenzothiophenes over NiMo/SBA-15 catalysts. AIChE J. 68 (5), 17577. https://doi.org/10.1002/aic.17577.

Weise, C.F., Falsig, H., Moses, P.G., Helveg, S., Brorson, M., Hansen, L.P., 2021. Single-atom Pt promotion of industrial Co-Mo-S catalysts for ultra-deep hydrodesulfurization. J. Catal. 403, 74–86. https://doi.org/10.1016/j.jcat.2021.03.008.

Wu, G.L., Yin, Y.C., Chen, W.B., Xin, F., Lu, Y.T., Qin, K., Zhang, L., Song, Y.X., Li, M.F., 2020. Catalytic kinetics for ultra-deep hydrodesulfurization of diesel. Chem. Eng. Sci. 214, 115446. https://doi.org/10.1016/j.ces.2019.115446.

Yin, Y., Chen, W., Wu, G., Xin, F., Qin, K., Lu, Y., Zhang, L., Li, M., 2021. Kinetics toward mechanism and real operation for ultra-deep hydrodesulfurization and hydrodenitrogenation of diesel. AIChE J. 67 (7), 17188. https://doi.org/10.1002/aic.17188.

Zheng, M., Zhao, L., Cao, L.Y., Gao, J.S., Xu, C., 2020. The combined DFT and microkinetics methods to investigate the favorite sulfur vacancies of Co(Ni)MoS_2 catalysts for maximizing HDS/HYDO selectivity. Appl. Catal. B Environ. 277, 119242. https://doi.org/10.1016/j.apcatb.2020.119242.

Zheng, P., Xiao, C.K., Cao, Z.K., Shi, Y., Wang, G., Duan, A.J., Xu, C., 2021. DFT insights into the hydrodesulfurization mechanisms of different sulfur-containing compounds over CoMoS active phase: effect of the brim and CUS sites. Chem. Eng. Sci. 231, 116311. https://doi.org/10.1016/j.ces.2020.116311.

Zhou, W., Liu, M., Zhang, Q., Wei, Q., Ding, S., Zhou, Y., 2017. Synthesis of NiMo catalysts supported on gallium-containing mesoporous Y zeolites with different gallium contents and their high activities in the hydrodesulfurization of 4,6-dimethyldibenzothiophene. ACS Catal. 7 (11), 7665–7679. https://doi.org/10.1021/acscatal.7b02705.

Zhou, W., Wei, Q., Zhou, Y., Liu, M., Ding, S., Yang, Q., 2018a. Hydrodesulfurization of 4,6-dimethyldibenzothiophene over NiMo sulfide catalysts supported on mesomicroporous Y zeolite with different mesopore sizes. Appl. Catal. B Environ. 238, 212–224. https://doi.org/10.1016/j.apcatb.2018.07.042.

Zhou, W., Yang, L., Liu, L., Chen, Z., Zhou, A., Zhang, Y., He, X., Shi, F., Zhao, Z., 2020. Synthesis of novel NiMo catalysts supported on highly ordered TiO_2-Al_2O_3 composites and their superior catalytic performance for 4,6-dimethyldibenzothiophene hydrodesulfurization. Appl. Catal. B Environ. 268, 118428. https://doi.org/10.1016/j.apcatb.2019.118428.

Zhou, W., Zhou, A., Zhang, Y., Zhang, C., Chen, Z., Liu, L., Zhou, Y., Wei, Q., Tao, X., 2019. Hydrodesulfurization of 4,6-dimethyldibenzothiophene over NiMo supported on Ga-modified Y zeolites catalysts. J. Catal. 374, 345–359. https://doi.org/10.1016/j.jcat.2019.05.013.

Zhou, W., Zhang, Q., Zhou, Y.S., Wei, Q., Du, L., Ding, S.J., Jiang, S.J., Zhang, Y.A., 2018b. Effects of Ga- and P-modified USY-based NiMoS catalysts on ultra-deep hydrodesulfurization for FCC diesels. Catal. Today 305, 171–181. https://doi.org/10.1016/j.cattod.2017.07.006.